An Inertial Navigation System
for a Mobile Robot

Billur Barshan and Hugh F. Durrant–Whyte
Robotics Research Group
Department of Engineering Science
University of Oxford
Oxford, OX1 3PJ United Kingdom

Abstract A low-cost, solid-state inertial navigation system (INS) for robotics applications is described. Error models for the inertial sensors are generated and included in an Extended Kalman Filter (EKF) for estimating the position and orientation of a moving robot vehicle. A solid-state gyroscope and an accelerometer have been evaluated. Without error compensation, the error in orientation is between 5–15°/min, but can be improved at least by a factor of 5 if an adequate error model is supplied. Similar error models have been developed for each axis of a solid-state triaxial accelerometer. Linear position estimation with accelerometers and tilt sensors is more susceptible to errors due to the double integration process involved in estimating position. With the system described here, the position drift rate is 1–3cm/sec, depending on the frequency of acceleration changes. The results show that with careful and detailed modelling of error sources, low cost inertial sensing systems can provide valuable position information.

1 Introduction

Inertial navigation systems (INS) have been widely used in aerospace applications [2, 3, 4] but have not been exploited much in the field of robotics. In [8], cooperation of inertial and visual information is investigated. Methods of extracting the motion and orientation of a robotic system from inertial information are derived theoretically but not directly implemented in a real system.

INS's are self-contained, nonradiating, nonjammable, dead-reckoning navigation systems which provide dynamic information through direct measurements. Fundamentally, gyros provide angular *rate* and accelerometers provide velocity *rate* information. Although the rate information is reliable over long periods of time, it must be integrated to provide orientation, linear position and velocity information. Thus, even very small errors in the rate information can cause an unbounded growth in the error of integrated measurements. One way of overcoming this problem is to use inertial sensors in conjunction with other absolute sensing mechanisms to periodically reset them. The approach taken in this work is to first incorporate in the system *apriori* information about the error characteristics to compensate for the errors before supplementing the INS with absolute sensing mechanisms.

In the following section, the hardware implementation of a robotic INS and its components are described. Section 3 focuses on generating error models for the sensors and testing them for adequacy of representation. In Section 4, the error models are exploited in an EKF for error compensation. The performance of the gyro is evaluated in Section 5 with and without an error model incorporated in the system. In Section 6, results of linear position estimation with the accelerometer are presented and discussed. Concluding remarks are made in Section 7.
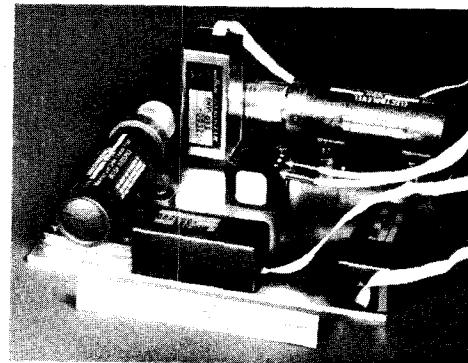

Figure 1: Picture of the INS package.

2 Description of the INS

In the Oxford AGV laboratory, an INS is under current development to aid in accomplishing the localization task in a 2-D environment which is not perfectly level. The system comprises three orthogonally-mounted rate gyros, a triaxial linear accelerometer manufactured by ENTRAN Devices Ltd., and two Electrolevel inclinometers (or tilt sensors) by TILT Measurement Ltd. all pictured in Figure 1.

The ENV-05S Gyrostar manufactured by Murata [7] is a small relatively inexpensive piezoelectric gyro developed for the automobile market with a maximum rate limit of ±90°/s. The accelerometer measures the *linear* acceleration of the robot along three mutually orthogonal axes on the robot frame. The measured value naturally incorporates the gravity vector that needs to be compensated for. The maximum range of the accelerometer along each axis is $\pm 2g = 19.62$ m/s^2. The device is centrally mounted on the vehicle such that its x and y axes are level with the vehicle platform and the z axis is orthogonal. Two orthogonally mounted tilt sensors measure small deviations of the vehicle platform up to ±10° from the horizontal $x - y$ plane with a discrimination of 1 arc.sec. The tilt information provided by these sensors is supplied to the accelerometer to cancel the gravity component projecting on each axis of the accelerometer. However, this can be accomplished only when the vehicle is stationary since all tilt sensors are inherently sensitive to acceler-
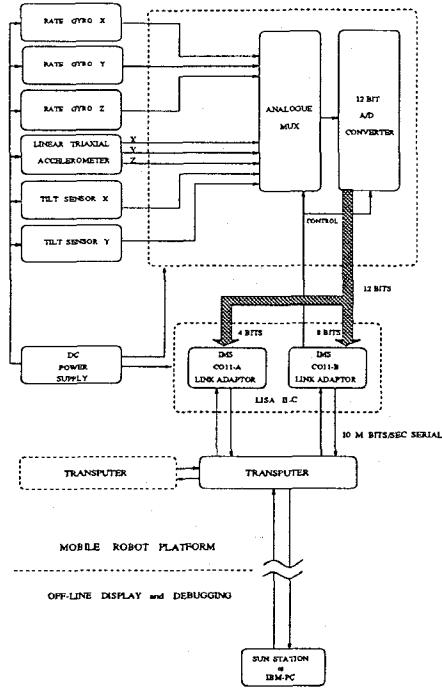
Figure 2: Hardware implementation of the INS.

Figure 3: Geometric configuration of the INS and the mobile robot equipped with it.

ation as well. When the vehicle comes to a stop, integrated rate from the gyros are reset the tilt sensors which directly provide angle information.

The block diagram for the hardware implementation of the inertial sensors is shown in Figure 2. Figure 3 illustrates the configuration of inertial sensors.

3 Constructing Error Models

Building error models for inertial sensors is motivated by an attempt to reduce the effect of unbounded position and orientation errors. Depending on how successful these models are, inertial sensors may possibly be used in an unaided mode or for longer durations on their own. Drift at the outputs of inertial sensors is the most important contributor to navigation system errors, and is mainly dependent upon the device technology. A detailed treatment of modelling aerospace INS's can be found in the first volume by Maybeck [6]. INS's developed for aerospace applications cannot be directly implemented on mobile ground vehicles since the scale, nature and parameters of the localization problem are different than in aerospace.

To develop an error model for the gyro, its output was recorded over long periods of time when subjected to zero input, i.e. the gyro was stationary on the laboratory bench. The result of this experiment over a period of 12 hours is shown in Figure 4. Ideally, the output for zero input would be a constant voltage level corresponding to the digital output of 2048 for a 12-bit A/D converter as shown by the thick solid horizontal line in the figure. The real output data is at a lower level than ideal at start-up, and the mean value gradually increases with time in an exponential fashion. The standard deviation of the output fluctuations is approximately $0.24°/s$. Repeatability of this result indicates that an apparently small time-varying bias is characteristic of this gyro. The time variation of the bias is attributed to thermal effects based on the observation that the gyro unit gradually
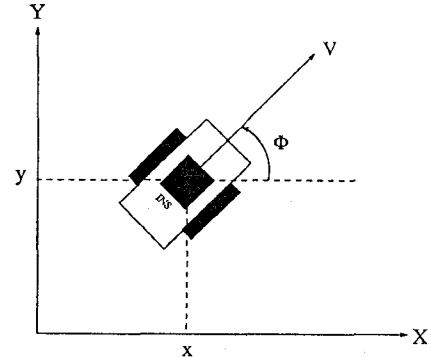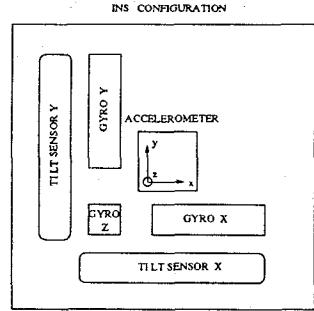

$$\text{A/D output} = 2048 \left(\frac{\dot{\phi}(k)}{90} + 1 \right)$$

ideal output

parameter fit

$$C_{1\dot{\phi}}(1 - e^{-\frac{t}{T_{\dot{\phi}}}}) + C_{2\dot{\phi}}$$
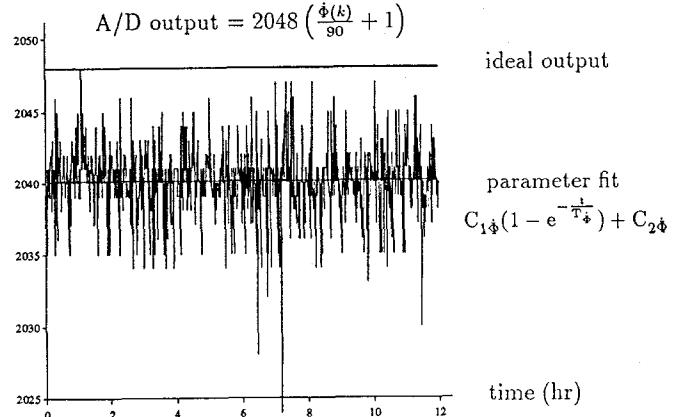
Figure 4: Digitized angular rate output of Gyrostar when subjected to zero input.

heats up during operation. Drift in the rate output of Gyrostar is about 30mV (1.35°/s.) 10 minutes after switching on and, provided there is no temperature change, about a further 10mV (0.45°/sec.) during the next 24 hours [7].

The same experiment to assess the drift has also been performed for each axis of the accelerometer. The error characteristics of each axis are of similar form but with differing parameters as shown in Figure 5. The error at the voltage output of each axis is characterized by a considerably large negative bias that drifts over time.

In the following, let $\epsilon(t)$ be the bias error associated with measuring the true value of a quantity of interest using inertial sensors. A nonlinear parametric model of the following form was fitted to the data from the gyros and the accelerometer using the

A/D output $= 2048 \left(\frac{a}{2g} + 1 \right)$
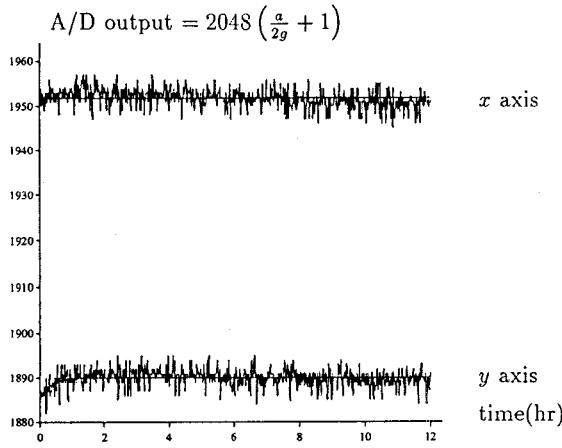
Figure 5: Digitized output of x and y axes of the ENTRAN accelerometer shown along with the fitted models of form $C_1(1 - e^{-\frac{t}{T}}) + C_2$.

Levenberg-Marquardt iterative least-squares fit method [9]:

$$\epsilon_{\text{model}}(t) = C_1 \left(1 - e^{-\frac{t}{T}} \right) + C_2 \tag{1}$$

where $\epsilon_{\text{model}}(t)$ is the fitted error model to the gyro output when zero input was applied, with parameters C_1, C_2, T to be tuned. Starting with reasonable initial guesses for the parameters, convergence to a local minimum is achieved within 5–10 iterations. The best fitting parameter values to the experimental data are tabulated in Table 1 for the inertial sensors which comply with this model.

Table 1 Drift model parameters

sensor:	C_1	C_2	T
gyro	$0.153°/s$	$-0.264°/s$	5.64min
acc-x	6.6cm/s^2	-148.7cm/s^2	16.3min
acc-y	2.7cm/s^2	-92.4cm/s^2	4.45min
acc-z	21.2cm/s^2	-56.9cm/s^2	138.5min

In general, a model fitted to experimental data is regarded as being adequate if the *residuals* from the fitted model constitute a white, zero-mean process. Hence, one can start with any reasonable model based on inspecting the original data and test its residuals for whiteness. If the test fails, the model can be further developed until the residuals pass the whiteness test. This implies that the test for the validity of any model is basically reduced to a test for whiteness. Following this route, the sufficiency of the above model in Equation 1 was tested for each sensor by applying a whiteness test to the residuals in the autocorrelation domain [1]. The positive outcome of this test demonstrates that the model in Equation 1 adequately represents the slowly varying bias errors. In the next section, the error models are exploited in an EKF to improve the performance of these sensors.

4 Implementing Error Models

The parametrized model of Equation 1 for the bias error can be represented by the following differential equation:

$$\dot{\epsilon}(t) = \frac{C_1 + C_2}{T} - \frac{1}{T} \epsilon(t) \tag{2}$$

with initial conditions $\epsilon(0){=}C_2$ and $\dot{\epsilon}(0){=}\frac{C_1}{T}$. After discretization, Equation 2 becomes

$$\epsilon(k+1) = \frac{T}{T + T_s} \epsilon(k) + \frac{T_s}{T + T_s} (C_1 + C_2) \tag{3}$$

with $\epsilon(0){=}C_2$. Due to its recursive nature, this difference equation is independent of start-up time but relies on a good estimate of the initial bias. The observations are

$$
\begin{aligned}
z_1(k) &= \dot{\theta}(k) + \epsilon_{\dot{\theta}}(k) + v_1(k) \\
z_2(k) &= \dot{\psi}(k) + \epsilon_{\dot{\psi}}(k) + v_2(k) \\
z_3(k) &= \dot{\Phi}(k) + \epsilon_{\dot{\Phi}}(k) + v_3(k) \\
z_4(k) &= \cos\psi.\cos\Phi.a_x(k) + \cos\psi.\sin\Phi.a_y(k) \\
&\quad - \sin\psi.g(k) + \epsilon_{a_x}(k) + v_4(k) \\
z_5(k) &= (\sin\theta.\sin\psi.\cos\Phi - \cos\theta.\sin\Phi)a_x(k) \\
&\quad + (\sin\theta.\sin\psi.\sin\Phi + \cos\theta.\cos\Phi)a_y(k) \\
&\quad + \sin\theta.\cos\psi.g(k) + \epsilon_{a_y}(k) + v_5(k) \\
z_6(k) &= (\cos\theta.\sin\psi.\cos\Phi + \sin\theta.\sin\Phi)a_x(k) \\
&\quad + (\cos\theta.\sin\psi.\sin\Phi - \sin\theta.\cos\Phi)a_y(k) \\
&\quad + \cos\theta.\cos\psi.g(k) + \epsilon_g(k) + v_6(k)
\end{aligned} \tag{4}
$$

Here, a_x, a_y and g are the accelerations of the robot in the *world* coordinate frame, related to the measured accelerations by a rotational transformation through θ, ψ, Φ around x, y and z axes respectively [5]. Equation 4 can be rewritten in matrix notation as:

$$\mathbf{z}(k) = \mathbf{h}[\mathbf{x}(k)] + \mathbf{v}(k) \tag{5}$$

where $\mathbf{x}(k)$ is the state vector and $\mathbf{v}(k)$ is a white measurement noise process vector.

Given the observations, the states that need to be estimated are the true values of orientation, angular rate, linear acceleration, velocity, position and the errors associated with them. Hence, the states of interest are augmented by Equation 3 for the sensors involved to estimate and compensate for the time-varying bias errors. The resulting state equations of the EKF in block matrix form are as follows:

$$
\begin{bmatrix} \mathbf{x}_{G_x}(k+1) \\ \mathbf{x}_{G_y}(k+1) \\ \mathbf{x}_{G_z}(k+1) \\ \mathbf{x}_{A_x}(k+1) \\ \mathbf{x}_{A_y}(k+1) \\ \mathbf{x}_{A_z}(k+1) \end{bmatrix} = \begin{bmatrix} \mathbf{F}_{G_x} & 0 & 0 & 0 & 0 & 0 \\ 0 & \mathbf{F}_{G_y} & 0 & 0 & 0 & 0 \\ 0 & 0 & \mathbf{F}_{G_z} & 0 & 0 & 0 \\ 0 & 0 & 0 & \mathbf{F}_{A_x} & 0 & 0 \\ 0 & 0 & 0 & 0 & \mathbf{F}_{A_y} & 0 \\ 0 & 0 & 0 & 0 & 0 & \mathbf{F}_{A_z} \end{bmatrix} \begin{bmatrix} \mathbf{x}_{G_x}(k) \\ \mathbf{x}_{G_y}(k) \\ \mathbf{x}_{G_z}(k) \\ \mathbf{x}_{A_x}(k) \\ \mathbf{x}_{A_y}(k) \\ \mathbf{x}_{A_z}(k) \end{bmatrix} + \begin{bmatrix} \mathbf{u}_{G_x} \\ \mathbf{u}_{G_y} \\ \mathbf{u}_{G_z} \\ \mathbf{u}_{A_x} \\ \mathbf{u}_{A_y} \\ \mathbf{u}_{A_z} \end{bmatrix}
$$

$$+ \mathbf{w}(k) \tag{6}$$

with $\quad \mathbf{F}_{G_x} \triangleq \begin{bmatrix} 1 & T_s & \frac{1}{2}T_s^2 & \frac{1}{6}T_s^3 & 0 \\ 0 & 1 & T_s & \frac{1}{2}T_s^2 & 0 \\ 0 & 0 & 1 & T_s & 0 \\ 0 & 0 & 0 & 1 & 0 \\ 0 & 0 & 0 & 0 & \frac{T_{\dot{\theta}}}{T_{\dot{\theta}}+T_s} \end{bmatrix}, \tag{7}$

$$\mathbf{F}_{A_x} \triangleq \begin{bmatrix} 1 & T_s & \frac{1}{2}T_s^2 & 0 \\ 0 & 1 & T_s & 0 \\ 0 & 0 & 1 & 0 \\ 0 & 0 & 0 & \frac{T_{a_x}}{T_{a_x}+T_s} \end{bmatrix}, \quad (8)$$

$$\mathbf{x}_{G_x}(k) \triangleq \begin{bmatrix} \Phi(k) \\ \dot{\Phi}(k) \\ \ddot{\Phi}(k) \\ \dddot{\Phi}(k) \\ \epsilon_\Phi(k) \\ \epsilon_{\dot\Phi}(k) \end{bmatrix}, \quad \mathbf{x}_{A_x}(k) \triangleq \begin{bmatrix} x(k) \\ v_x(k) \\ a_x(k) \\ \epsilon_{a_x}(k) \end{bmatrix}, \quad (9)$$

$$\mathbf{u}_{G_x} \triangleq \begin{bmatrix} 0 \\ 0 \\ 0 \\ 0 \\ \frac{T_s(C_{1\dot\Phi}+C_{2\dot\Phi})}{T_{\dot\Phi}+T_s} \end{bmatrix} \text{ and } \mathbf{u}_{A_x} \triangleq \begin{bmatrix} 0 \\ 0 \\ 0 \\ \frac{T_s(C_{1a_x}+C_{2a_x})}{T_{a_x}+T_s} \end{bmatrix} \quad (10)$$

The remaining block matrices and vectors in Equation 6 have very similar definitions to those in Equations 7– 10 but with the corresponding error model parameters substituted [10]. More compactly, Equation 6 can be rewritten as:

$$\mathbf{x}(k+1) = \mathbf{F}\mathbf{x}(k) + \mathbf{u} + \mathbf{w}(k) \quad (11)$$

Note that the state transition is *linear* unlike the nonlinear measurements described by Equation 5. The first four states are the *true* values of the orientation and its derivatives, and the next two states constitute the error model for the gyroscope. This part of the filter has a constant $\dddot{\Phi}(k)$ structure augmented by the error model. Lower-order filters have been implemented but shown to have a delay and much ringing in their unit-step response. With this higher-order model, the filter is able to track abrupt changes in angular velocity very closely as will be shown in the next section. The remaining states of the filter correspond to the true values of position, velocity and acceleration in the world frame, plus the error states for measuring acceleration. One interesting point to note is that for each different sensor, the error states are coupled to their relevant true states only through the observation equations and not by the structure of the state transition matrix $\mathbf{F}$.

The EKF structure in Equations 5 and 11 has been implemented in real time on an INMOS-T805 transputer network where a minimum sampling interval of T_s=90 ms. is achieved. The gyro has been mounted on a rotating platform whose angular velocity and orientation can be accurately controlled and measured. For comparison purposes, the platform velocity and orientation are taken to be the "true" values of these quantities. Initial estimates of the bias errors are made to initialize the filter by averaging the output of each inertial sensor over a large number of samples when the robot is not in motion. As data is collected by the inertial sensors, the EKF running in parallel filters the measurements and provides estimates of the quantities of interest for the mobile robot.

5   Performance of the Gyro

To determine the adequacy of the error models, the system performance with no assumed error model is compared to the performance when the error model in Equation 1 is incorporated in the EKF for the gyro. The results when zero-input was applied to the Gyrostar are shown in Figure 6 over a duration of five minutes. At the end of the experiment, the integrated gyro rate output was −57.1°/s., whereas the compensated and filtered output was +3.72°, having had an overall maximum deviation
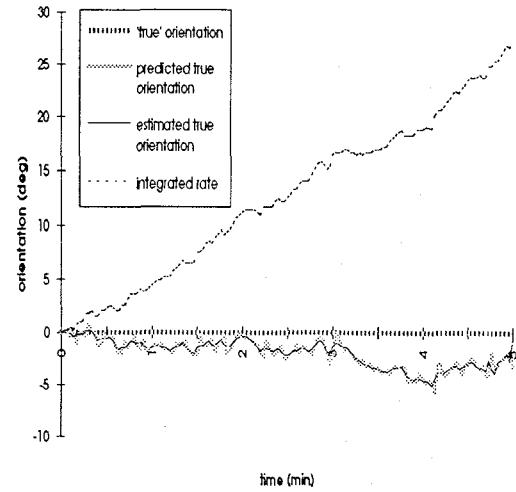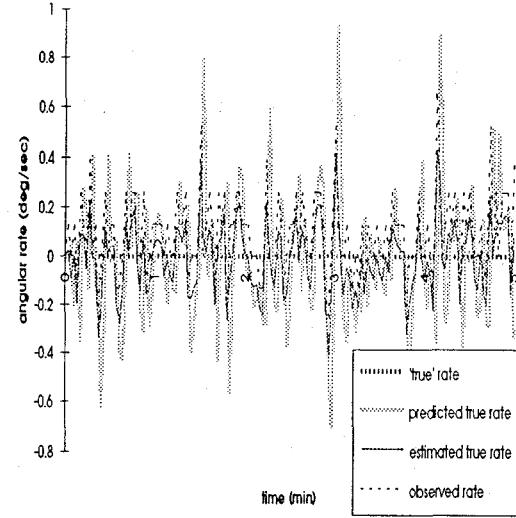

Figure 6: Angular rate and orientation of Gyrostar for zero-input case.

of +7.40° from the true value. The improvement was by a factor of 7.7. Figure 7 illustrates the angular rate and position of the Gyrostar when non-zero input was applied for a total duration of five minutes. A new angular rate $-25 \le \dot{\Phi} \le 25°/s$. is randomly generated every 30 s. and applied to the gyro. The true values and the erroneous observations are displayed along with the filter results. At the end of the experiment, the integrated rate output exhibited an error of −42.5° whereas the filtered estimate was +10.7°. Both the gyro rate output and the filtered rate output were accurate within ±1.5°/s. at the end of the experiment.
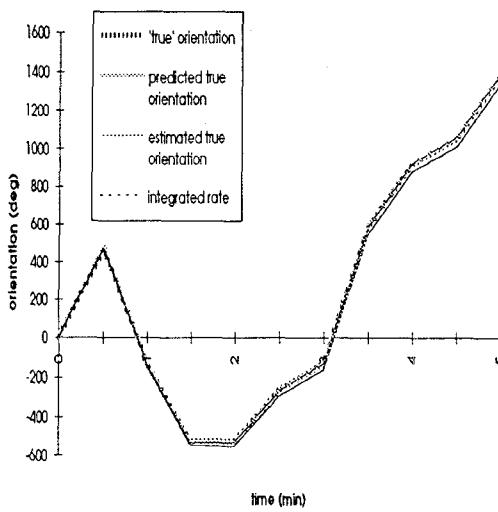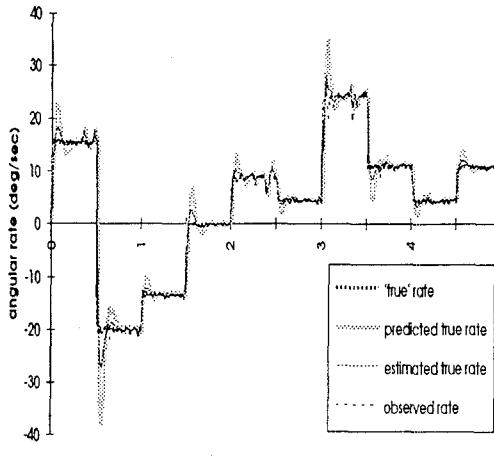
Figure 7: Angular rate and position of Gyrostar when non-zero input was applied.

6 Accelerometer Evaluation

To evaluate the accelerometer for position estimation, a simple experiment was designed: The robot platform was accelerated and decelerated over a distance of 30 cm. along its x axis in the forward and backward directions. The results from the accelerometer is illustrated in Figure 8. In Figure 8(a), real data from the accelerometer is shown in dotted line, EKF estimate is in solid line.

The dashed line corresponds to the output of the tilt sensor x functioning as an accelerometer for comparison purposes. In Figures 8(b) and (c), solid lines indicate EKF estimates of velocity and position along the x axis. The dashed lines correspond to the numerical integration of the tilt sensor output. At the end of the experiment, position estimation using the accelerometer was erroneous by -15.3 cm. Although this example is a case where the drift on the accelerometer was relatively small, the position estimation error can easily exceed 60-80 cm. over a duration of 10 sec. Position estimation with information from accelerometers and tilt sensors is more susceptible to errors due to the double integration process. With the system described here, the position drift rate is between 1-8 cm/sec., necessitating the fusion of information from absolute sensing mechanisms.
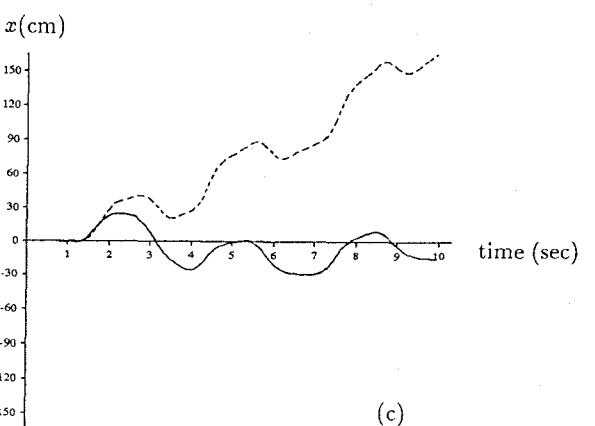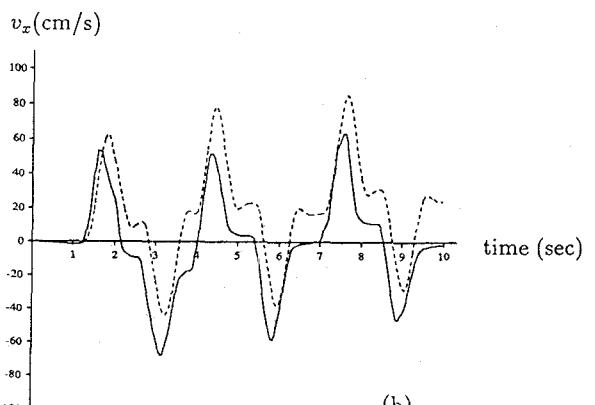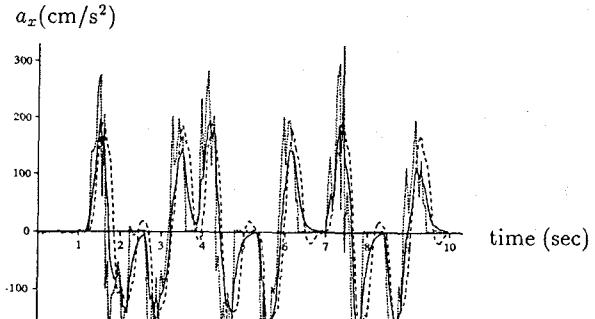

Figure 8: Position estimation with the accelerometer and tilt sensors.

7 Conclusion

The results demonstrate that the Gyrostar provides accurate localization of a mobile robot only if an adequate error model is generated and supplied to the EKF. The model reduces the angular position error at least by a factor of 5. With the resulting accuracy, it is still necessary to reset the error with absolute sensing information at regular intervals. The gyro with the given model would operate particularly well in environments where the ambient temperature is controlled. Linear position estimation with information from accelerometers and tilt sensors was performed. The results show that with careful and detailed

modelling of error sources, low cost inertial sensing systems can provide valuable position information. The error analysis and fusion of information for this system is under further development. Current research also involves integrating this INS with other sensing mechanisms.

8 Acknowledgements

References

[1] B. Barshan and H. F. Durrant-Whyte. Evaluation of a solid-state gyroscope for robotics applications. Technical report, Robotics Research Group, Oxford University, 19 Parks Road, Oxford, October 1992. Report No. OUEL 1957/92.

[2] C. T. Leondes, editor. *Theory and Applications of Kalman Filtering*. Technical Editing and Reproduction Lmtd., London, 1970. Sponsored by NATO Advisory Group for Aerospace Research and Development.

[3] D. A. Mackenzie. *Inventing Accuracy: A Historical Sociology of Nuclear Missile Guidance*. MIT Press, Cambridge, MA, London, 1990.

[4] I. J. Cox and G. T. Wilfong, editor. *Autonomous Robot Vehicles*. Springer-Verlag, New York, 1990. Section on Inertial Navigation edited by M. M. Kuritsky and M. S. Goldstein.

[5] J. J. Craig. *Introduction to Robotics: Mechanics and Control*. Addison-Wesley, Reading, MA, 2. edition, 1989.

[6] P. S. Maybeck. *Stochastic Models, Estimation, and Control*, volume I,II,III. Academic Press, New York, 1979.

[7] T. Shelley and J. Barrett. Vibrating gyro to keep cars on route. *Eureka on Campus, Engineering Materials and Design*, 4(2):17, Spring 1992.

[8] T. Viéville and O. D. Faugeras. *Cooperation of the Inertial and Visual Systems*, volume F63 of *NATO ASI Series*, pages 339–350. Springer-Verlag, Berlin, Heidelberg, 59. edition, 1990. in Traditional and Non-Traditional Robotic Sensors edited by T. C. Henderson.

[9] W. H. Press, B. P. Flannery, S. A. Teukolsky and W. T. Vetterling. *Numerical Recipes in C*, pages 540–547. Cambridge University Press, Cambridge, U.K., 1988.

[10] Y. Bar-Shalom and T. E. Fortmann. *Tracking and Data Association*. Academic Press, New York, 1988.